Effect of morphology and hydrophobization of MoS2 microparticles on the stability of poly-α-olefins lubricants

M Z Saidi , H Akram, O Achak , C El Moujahid , A El Mouakibi, N. Canilho, C. Delgado-Sánchez, A. Celzard, Vanessa Fierro, Andreea Pasc, et al.

Contents lists available at ScienceDirect

Colloids and Surfaces A: Physicochemical and Engineering Aspects

journal homepage: www.elsevier.com

Effect of morphology and hydrophobization of MoS_2 microparticles on the stability of poly-α-olefins lubricants

M.Z. Saidi [a], H. Akram [a,*], O. Achak [a], C. El moujahid [a], A. El Mouakibi [c], N. Canilho [b], C. Delgado-Sánchez [d], A. Celzard [d], V. Fierro [d], A. Pasc [b,*], T. Chafik [a]

[a] Laboratoire de Génie Chimique et Valorisation des Ressources, Faculté des Sciences et Techniques de Tanger, Université Abdelmalek Essâadi, B.P. 416, Tanger, Morocco
[b] L2CM UMR CNRS 7053, Université de Lorraine, F-54506, Vandoeuvre-lès-Nancy, France
[c] Guepo GmbH Chemie und Technik, Kehl, Germany
[d] Institut Jean Lamour, UMR 7198, CNRS – Université de Lorraine, ENSTIB, 27 rue Philippe Séguin, BP 21042, 88051 Epinal cedex 9, France

ARTICLE INFO

Keywords:
MoS_2 particles
Nano-sdditives
Poly-α-olefin base oil
Surface hydrophobization
Suspension stability

ABSTRACT

The use of MoS_2 nanoparticles as additive to lubricating oils is restricted by their low stability in oily media, which limits their use despite the enormous benefits associated with their intrinsic properties in terms of reduction of friction and wear coefficients. In this context, we investigated the effect of morphologies (platelets *vs* spheres) and surface functionalization of nanoparticles on the stability of their suspensions in poly-α-olefins (PAO) with various viscosities, which are base oils used in wind turbines. The particles were characterized by XRD, FTIR, scanning electron microscopy, atomic force microscopy and dynamic light scattering, and the stability of the resultant formulations was followed by optical (non-contact) measurements. It was found that the dispersions had similar stability despite the larger size of platelet-like particles compared to spherical ones (1–5 μm *vs* 600–800 nm). The dispersibility could be increased through grafting of alkylsilane on the surface defects (the longer the alkyl chain, the more stable the formulation) and with the increase of the oil kinematic viscosity (from 34 to 1705 cps at 25 °C).

1. Introduction

Fluid lubricants are used in almost every moving mechanical system, particularly in transmission and rotational bearings, in order to reduce friction and wear, and thus to ensure longer durability and less frequent equipment maintenance.

The development of advanced lubricants, operating over a broad range of temperature as well as in humid and oxidizing conditions, remains challenging. Indeed, lubricant properties should neither be altered by solidification at low temperature nor by the drop of viscosity at high temperature [1]. To do so, advanced additives with antifriction and antiwear properties have been developed, among which MoS_2 remains the most widely studied [2]. The interest of those particles is essentially due to their layered hexagonal crystal structure, with strong intra-layer covalent bonds and weak inter-layer van der Waals bonds, which decrease friction between the interfaces [3].

Moreover, it was previously reported that embedding those crystalline domains within amorphous MoS_2 structures might further improve frictional properties [4]. This was explained by the facilitated exfoliation of the external layers of the particles due to the defects of the amorphous matrix, as well as by the increased contact area of the microcrystalline domains of the additives compared to perfectly crystallized particles [5]. On the other hand, an increase of the contact surface area and hence of the frictional properties can be reached by decreasing the size of the particles down to the nanoscale. This could be explained by the fact that the increase of surface area leads to an increase of surface energy and thus to a global enhancement of the adsorption of nano-additives on metal surfaces [6]. Besides, the small size of the particles should insure higher dispersion stability, which is of paramount importance for proper nano-lubricant formulations. Another parameter that may influence both frictional properties and stability of the oily dispersions is the shape of the particles (*i.e.*, platelet-like or spheres) [7]. Lubrication mechanism involving platelet-like particles is indeed characterized by their sliding and shearing due to the van der Waals forces between the lamellar layers, which improve their tribological performances [8]. In the case of spherical particles, the lubrication efficiency is attributed to their chemical inertness, as well as to

* Corresponding authors.
Email addresses: akramhanane@yahoo.fr (H. Akram); andreea.pasc@univ-lorraine.fr (A. Pasc)

https://doi.org/10.1016/j.colsurfa.2019.04.003
Received 15 February 2019; Received in revised form 23 March 2019; Accepted 6 April 2019
Available online xxx
0927-7757/

rolling, sliding and exfoliation mechanisms [6,9]. Another difference between the two friction mechanisms as a function of shape is the pressure contact between the particles and the contact zone. Spherical particles exhibit a point contact with the counter-surface, while platelets have a planar contact [10]. It is thus difficult to predict the friction properties only based on particle's shape. Although layered spherical particles are the most common shapes in lubricant formulations, some studies reported that platelet-like particles were able to induce similar effect.

MoS_2 nanoparticles with various sizes, morphologies, and structures can be prepared by different techniques such as solvothermal process [11], hydrothermal process [12], or chemical vapor deposition (CVD) [13]. Nevertheless, whatever their shape, the preparation of lubricant nano-additives needs to overcome the crucial problem of sedimentation in oil. Especially in the case of wind turbines for example, since a shutdown for a few hours or days annually is necessary either because of inappropriate airflow (wind too weak or too strong) or because of maintenance and repair [14]. Hence, one of the key points is to enhance the dispersibility and the stability of the formulations, and thus the tribological properties of nano-lubricants [15,16]. For this purpose, various dispersants could be used to increase the stability of those kinds of formulations, as seen in Table 1.

Indeed, dispersing agents have been found effective in improving the stability of nanoparticles dispersed in nonpolar media, the hydrophilic part of the dispersing agent either physisorbing at the surface of the nanoparticles or reacting with surface defects and thus reducing their surface energy and consequently their tendency to agglomerate. Meanwhile, the hydrophobic part might improve the compatibility between solid-liquid interfaces and thus improve the dispersion in nonpolar organic solvents. For instance, the functionalization of IF-WS_2 nanoparticles with alkoxysilane groups (*i.e.,* octadecyl-, dodecyl-) allowed reducing the reactive sites exposed on the surface of the nanoparticles and thus led to more stable dispersions in oily suspensions [28]. Similar results were obtained by Kumar et al [27] who showed that the functionalization of micro-MoS_2 particles by trichlorooctadecylsilane permitted stable dispersions in base oils as well as significant improvement of anti-wear, anti-friction and extreme-pressure properties. So far, our previous work showed that alkyl-silane groups increased the dispersability of MoS_2 particles in various poly-α-olefins PAO base oils [29,30]. Beyond alkyl-silane groups, other coatings have been found to be effective in improving hydrophobicity (*i.e.* melamine-formaldehyde with [31] or without [32,33] vulcanized silicon rubber) or dispersibility of MoS_2 particles (long chain alkyl-thiol [17,20], oleylamine [19] or sodium dodecylsulfate [21],).

In this context, we investigated the stability of MoS_2 microparticles in four PAO base oils of various viscosities. Particular attention was paid to the influence of the alkyl chain length on the dispersibility of the resultant additives. This issue was addressed for two kinds of particles, having either a platelet-like (**p-MoS_2**) or a spherical morphology (**s-MoS_2**), the latter being synthesized by the solvothermal method. As reported elsewhere, the latter limits the use of chemicals and the production of solid waste, and also allows energy savings [11]. Regarding environmental impacts, in addition to the aforementioned advantages, the use of Life Cycle Assessment approach revealed that the adopted solvothermal method is "greener" than the most relevant preparation methods reported in literature [34].

2. Experimental part

2.1. Materials

All reagents were purchased from Sigma Aldrich and used without further purification. Platelet-like MoS_2 particles were also purchased from Sigma-Aldrich under the reference 804169. Contrary to the provider's specifications, the sample contained less than 10% of 50 nm particles, the rest being platelets of about 1–5 μm (see SEM characterisation). PAO base oils were graciously provided by Chevron Phillips Chemical Company LP. Details on their physico-chemical properties are given in table SI1.

2.1.1. Synthesis of MoS_2 microparticles (s-MoS_2)

In a typical solvothermal procedure, [11] 0.10 g of $(NH_4)_6Mo_7O_{24}.4H_2O$, 0.04 g of S, 0.75 g of $LiOH.H_2O$, 0.05 g of $(NH_4)_2CO_3$ and 6 mL of $N_2H_4.H_2O$ were introduced in a lab-made Teflon-lined stainless steel autoclave. Ethylenediamine was then added to fill up to 80% of the total volume of the autoclave (190 mL). The solvothermal treatment was performed at 190 °C for 24 h. The autoclave was then cooled down to room temperature. The black product was recovered by centrifugation and washed with acetone and distilled water. The resultant powder was dried under vacuum at 75 °C for 3 h. The yield was quasi-quantitative.

2.1.2. Silane coating of MoS_2 nanoparticles

Two silane derivatives, octadecyltrichlorosilane (ODTS, $C_{18}H_{37}SiCl_3$) and octyltrichlorosilane (OTS, $C_8H_{17}SiCl_3$), were used to hydrophobize the surface of MoS_2 particles by adding 1 wt.% of alkyltrichlorosilane (ODTS or OTS) to poly-α-olefin oil containing 0.1 wt.% of MoS_2 particles. The mixture was sonicated (using a 200 W Sonopuls HD 2200 device used at 45% of its nominal power) for 15 min, and then magnetically stirred for 2 h at room temperature.

Table 1
Overview of previously reported formulations of MoS_2 particles as additives in lubricant oils: morphology, synthesis, dispersing agents and stability.

Morphology of MoS_2	Synthesis method	Average size	Surfactant/ dispersant	Lubricant	Stability	Ref.
nanosheets	Hydrothermal	–	Octadecanethiol	polyol ester	11 days	[17]
Nanosheets	– (Sigma-Aldrich)	–	Polyhydroxy-polyglycerol	PBS buffers	1 week	[18]
Nanosheets	Solvothermal method	Lateral size 20-30 nm	Oleylamine	Paraffin oil	7 days	[19]
Nanosheets	Reverse microemulsion	100 nm	Dodecanthiol	Base olefin	24 h	[20]
Platelets	– (Sisco Research Laboratories Pvt)	90 nm	Sodium Dodecyl Sulfate	Coconut oil Paraffin oil	100 days	[21]
Nanospheres	Wet chemical synthesis	20 nm	Sodium Dodecylsulfate	SAE engine oil	–	[22]
Nanoparticles	Ball milling	100-500 nm	Lecithin	Poly-α-olefin base oil	–	[23]
Nanoparticles	– (M. K Impex)	50 nm	APTMS, SPAN 80, OTS, PTS, PTCS	500 N-Base oil	15 days	[24]
flower like	Solvothermal	150/350 nm	Succinimide	Blend of PAO4 and PAO40	–	[25]
Microspheres	Solvothermal	1-3 μm	Cyanex 301	Liquide paraffin	–	[26]
microlayered particles	– (Sigma-Aldrich)	2 μm	Trichloro-octadecylsilane	mineral base oil N-150	28 days	[27]

APTMS: Aminopropyltrimethoxysilane; SPAN 80: Sorbital monooleate; OTS: Octadecyltrimethoxysilane; PTS: Perfluorodecyltriethoxy-silane. PTCS: Perfluorooctyltrichlorosilane.

2.2. Characterization methods

2.2.1. X-ray diffraction (XRD)

The phase purity and crystalline structure of the MoS_2 particles were studied by XRD using a Bruker D8 ADVANCE ECO diffractometer with Cu/Kα radiation (λ = 0.154 nm) operating at 35 kV and 35 mA. The Bragg's angles between 4° and 80° were scanned at a rate of 0.04°/s.

2.2.2. Scanning electron microscopy (SEM)

The morphology of the MoS_2 samples was observed with a Hirox SH-4000 M electron microscope equipped with an energy-dispersive X-ray (EDX) spectrometer.

2.2.3. Atomic force microscopy (AFM)

AFM observations were performed on a Nanosurf FlexAFM C3000 operating at room temperature at 150.97 kHz and 800 mV, in phase contrast mode, using a NCLR cantilever. The AFM specimens were prepared by dispersing a small amount of MoS_2 powder in ethanol, placing one drop of this dispersion on a lacey Mica film and allowing solvent evaporation.

2.2.4. Fourier-transform infrared spectroscopy (FTIR)

FTIR analysis was performed on a Jasco 410 spectrometer at a spectral resolution of 4 cm^{-1}. 2 wt.% of MoS_2 powder was thoroughly ground and mixed with dry KBr and pressed into disks before analysis.

2.2.5. Dynamic light scattering (DLS)

The size distribution of the particles was measured by DLS on a Malvern Zetasizer 300HSA operating at an angle of 90°. The samples were diluted before analysis, due to the opacity of the as-prepared suspensions. The values of viscosity at 25 °C were settled at 34 cps for PAO 4, 66 cps for PAO6, and 97 cps for PAO 8. Measurements in PAO65 were not possible due to the too high viscosity of this oil (1705 cps at 25 °C), which prevented the movement of the particles and hence the measurement of their sizes.

2.2.6. Multiple light scattering

The stability of the suspensions was determined using an optical analyzer (TURBISCAN LAB from Formulaction, L'Union, France), based on a light-scattering detection method. Before measurements, the suspensions were submitted to a continuous high-intensity ultrasound probe of 400 W used at 20% of its maximum power during 3 min. Then, they were poured into special cylindrical glass vials of height and internal diameter of about 55 and 25 mm, respectively, which were immediately installed in the instrument, previously conditioned at 25 °C. The stability of the suspensions was analyzed based on transmission (T) and backscattering (BS) profiles as responses to applied pulses from a near-infrared (λ = 850 nm) laser diode. The mobile detection head scanned the sample tube along its vertical axis every 3 min during the first 24 h, every 30 min during the next 48 h and every 3 h during the next 120 h (8 days in total), gathering T and BS data at sample heights separated by 20 μm. For better detecting the various destabilization phenomena that may occur in the present suspensions as a function of time, the T and BS profiles were analyzed in Delta (Δ) mode. In this mode, one of the profiles (by default, the first one) was used as a reference corresponding to the initial state of the suspensions. This profile was then subtracted to all the other ones, thus emphasizing the changes. Doing so, it is expected that when some destabilization phenomenon takes place in the suspension, the delta transmission (ΔT) and the delta backscattering (ΔBS) vary along the height of the suspension as well as a function of time. If the suspension was completely stable, no change of ΔT and ΔBS would be observed.

Another tool for studying the stability of suspensions can also be used, called Turbiscan Stability Index (TSI). Since any destabilization phenomenon occurring in a suspension has an effect on T and/or BS signal intensities during time, the formulation with the highest intensity variation is therefore the least stable. The TSI simply sums up the evolution of T or BS light at every measured position (*h*), based on a scan-to-scan difference, over total sample height (*H*), and thus reads:

$$TSI = \frac{\sum_{h} \left| scan_i(h) - scan_{i-1}(h) \right|}{H} \quad (1)$$

The TSI is thus a single dimensionless parameter allowing the rapid comparison and characterization of the physical stability of different formulations. The lower the changes of transmission and/or backscattering intensity, the lower its value and hence the more stable is the formulation. According to the manufacturer of the Turbiscan device, the TSI scale is such that values from 0 to 0.5, 0.5–1, 1–3, 3–10 and above 10 correspond to extremely stable, stable, moderately stable, poorly stable and unstable formulations, respectively. Destabilization can be seen by naked eye for TSI typically above 3. Finally, destabilization kinetics can be obtained by plotting the TSI values as a function of time.

3. Results and discussion

3.1. Bare MoS_2 particles

The morphology of MoS_2 particles was investigated by SEM and AFM (Fig. 1). Both techniques showed that MoS_2 particles prepared by the solvothermal method displays a polydisperse size distribution centered on about 800 nm. The commercially available particles, **p-MoS_2** (purchased from Sigma-Aldrich, ref. 804169) appeared on SEM micrographs as disordered sheets with obvious tendency to aggregation. AFM cliché confirmed the lamellar morphology of **p-MoS_2** and clearly showed the staking of layers of a few microns in thickness.

The crystalinity and phase purity of microparticles were assessed by XRD. Fig. 2 displays the XRD patterns of spherical and platelet-like MoS_2 particles and, for comparison, the one of 2H-MoS_2 in its most stable hexagonal crystalline structure. The XRD pattern of **s-MoS_2** shows three broad peaks at 15.5°, 34° and 42° that might be ascribed to the 002, 100 and 103 reflections characteristic of MoS_2 hexagonal structure. The pattern of indicates a poorly crystalline molybdenum disulfide structure and the lack of long-range ordering. On the contrary, the XRD pattern of platelet-like particles, **p-MoS_2**, is characteristic of a highly ordered hexagonal MoS_2 structure, similar to the one of 2H-MoS_2.

EDX analysis allowed verifying the chemical composition of the particles. The as-synthesized spheres exhibited only two peaks corresponding to the presence of only molybdenum and sulfur (Fig. SI3), with an atomic ratio Mo:S of 1:1.9 (Table S2). For **p-MoS_2**, EDX data revealed the presence of oxygen in addition to molybdenum and sulfur with atomic ratios Mo:S of 1: 1.38 and Mo:O of 1:0.4 (Fig. S1 (B), Table S3).

Further characterization of the particles was achieved from FTIR. Fig. 3 (left) shows the IR spectra of **s-MoS_2** spheres. The band at 470 cm^{-1} can be assigned to the stretching vibrations of Mo-S [17]. The band at 534 cm^{-1} is assigned to bridged S_2^{2-} species, while the bands at 636, 1050, 1132 and 1451 cm^{-1} can be ascribed to sulfates. [11,35] A strong band at 799 cm^{-1} was also observed and can be due to the symmetrical and asymmetrical stretching vibrations of *cis* dioxo group MoO_2^{2+} [36]. The presence of these bands confirms that the synthesized molybdenum disulfide oxidized in contact with air, and/or hydrolyzed. The bands observed at 1508, 1576, 1636 cm^{-1} are due to the presence of ammonium ions resulting either from the precursor or elec-

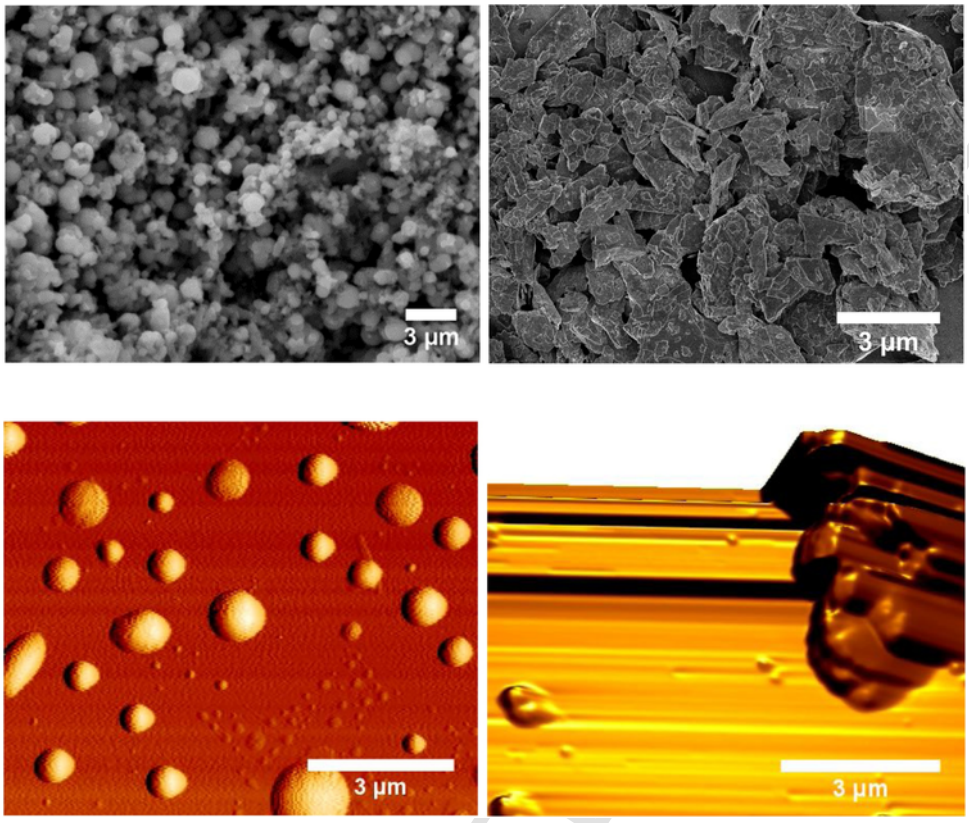

Fig. 1. SEM (top) and AFM (down) images of MoS_2 particles revealing two morphologies: spheres for **s-MoS_2** (left) and platelets-like for **p-MoS_2** (right).

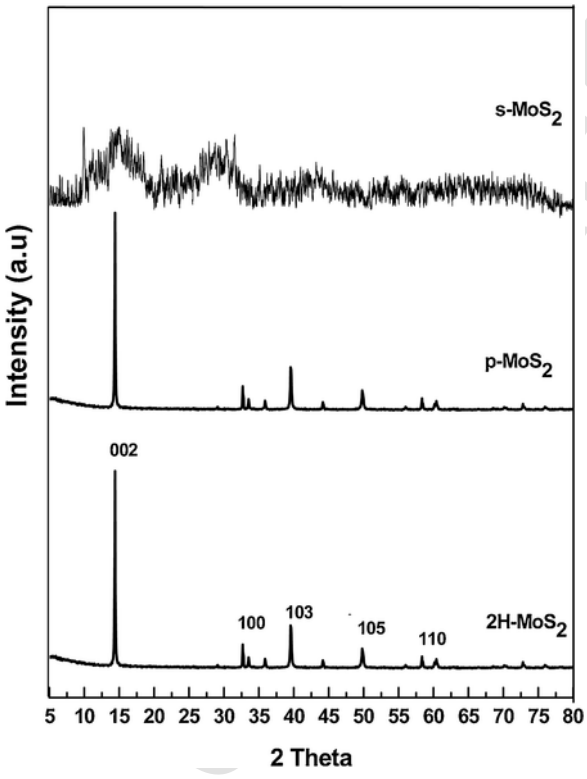

Fig. 2. XRD patterns showing poorly crystalline spherical **s-MoS_2** and highly crystalline platelet-like **p-MoS_2** particles as compared with 2H-MoS_2 in the most stable hexagonal structure.

trolyte decomposition. [37] The broad bands observed between 3200 and 3500 cm^{-1} might be due to adsorbed H_2O. [20]

The IR spectra of **p-MoS_2** particles (Fig. 3 right) show the presence of IR bands of low intensity at 468 cm^{-1} attributed to Mo-S bond. [11] Other bands at 1128 and 1395 cm^{-1} can be assigned to sulfate species [38]. The band of low intensity appearing at 1644 cm^{-1} and the broad peak observed about 3441 cm^{-1} were attributed to O–H group [39].

The appearance of hydroxyl groups indicated by the bands between 3200 and 3500 cm^{-1} on the IR spectra of both kinds of nanoparticles studied, **s-MoS_2** and **p-MoS_2**, might be due to the adsorption of water molecules on the surface of these particles during their exposure to air, which makes their surface more hydrophilic and therefore their suspension more unstable in oily media.

3.2. *Functionalized MoS_2 particles*

The functionalization of particles with alkyltrichlorosilane (OTS (-C_8) and ODTS (-C_{18})) (Fig. 4) was followed by FTIR (Fig. 3). The two new bands in the 2850-2950 cm^{-1} region appeared for both materials upon functionalization and were assigned to the symmetric and asymmetric stretching vibrations of methylene groups [28] from the dispersants (Fig. 3). The IR bands located at 1460 and 1374 cm^{-1} were attributed to modified p-MoS_2, whereas the band at 1365 cm^{-1} correspond to s-MoS_2 are attributed to Si-C vibrations. [40] A new band characteristic of Si-O vibration also appeared at around 1060 cm^{-1} confirming once again the grafting of alkoxisilane onto MoS_2 particles [41]. One can also note the disappearance of the bands between 3200 and 3500 cm^{-1} attributed to the hydroxyl groups of adsorbed water vapor, and a slight displacement in the others peaks after chemical modification of the nanoparticle surface, which suggests that the silane groups attached to the surface of the synthesized MoS_2 and replaced the water molecules adsorbed by the alkyl silane groups. This phenomenon was previously

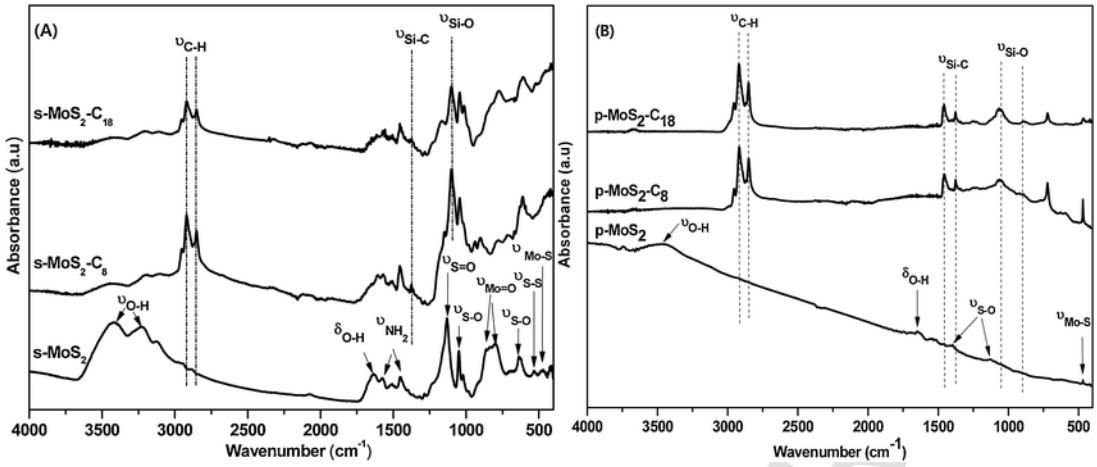

Fig. 3. IR spectra of **s-MoS_2** (A) and **p-MoS_2** (B) particles before and after functionalization with trichloroalkoxilsilane (OTS (-C_8) and ODTS (-C_{18})).

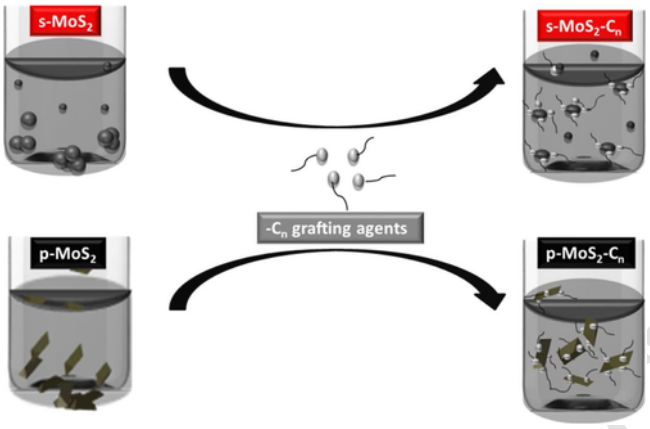

Fig. 4. Schematic representation of the surface modification of MoS_2 particles with alkyl-silanes dispersants.

reported for WS_2 nanoparticles and it was associated to the defects of the surface [28].

A first evaluation of the functionalization impact on particles aggregation was assessed by dynamic light scattering measurements. The particle size distribution of **s-MoS_2** particles was determined in three lubricating poly-α-olefin oils (PAO4, PAO6 and PAO8), whose physico-chemical properties are given in Table SI1. Bare synthesized particles showed a unimodal size distribution centered on 1002, 908 and 1287 nm in PAO4, PAO6 and PAO8, respectively. The addition of 1 wt.% of dispersant (-C_8 or –C_{18}) significantly reduced the average size of those aggregates and improved their distributions, as shown in Fig. 5. For instance, with -C_8, the size distribution was centered on 796, 858 and 785 nm in PAO4, PAO6 and PAO8 oils, respectively. The use of a more hydrophobic grafting agent, such as ODTS (-C_{18}), led to even smaller sizes of 658, 716 and 657 nm in the same oils, respectively. These results demonstrate the dispersing power of alkyl-silanes and especially the positive effect of the hydrocarbon chain length for improving the dispersibility of these nanoparticles in PAO base oils.

Further evaluation of the functionalization impact on particles aggregation and sedimentation and thus on the stability of the formulations was assessed by multiple-light scattering using the Turbiscan device. The instabilities that can be encountered in the suspensions at room temperature can be observed in the typical Δ-transmission (ΔT) and Δ-backscattering (ΔBS) profiles shown in Fig. 6 as a function of time (corresponding to curves of different colours from blue at instant 0 to red at 8 days) and as a function of height (corresponding to the horizontal axis). The sedimentation of the particles can be identified at the bottom of the sample holder (typically at less than 2 mm of height from the bottom in this example) by a positive peak of ΔBS that becomes higher and broader with time. The process of clarification can be observed in the rest of the glass tube. It begins with a progressive decrease in the ΔBS profile and after some time, the light can pass throughout the suspension and the T detector becomes able to record the ΔT profile. Once transmitted light is detected, the BS signal is no more studied because it interferes with the reflection of the light going across the sample.

Finally, a third phenomenon of destabilisation can be observed in the clarification regime; it is detected as a little decrease in ΔT signal and an increase in the ΔBS that might be due to the agglomeration of the particles.

The Turbiscan Stability Index (TSI) is related to the variation rate of T and BS intensities with respect to the initial ones. The more they change, the higher is the TSI and the less stable is the suspension. The curves of TSI of all suspensions at room temperature are shown in Fig. 7 as a function of time. As a general trend, the TSI decreased with the

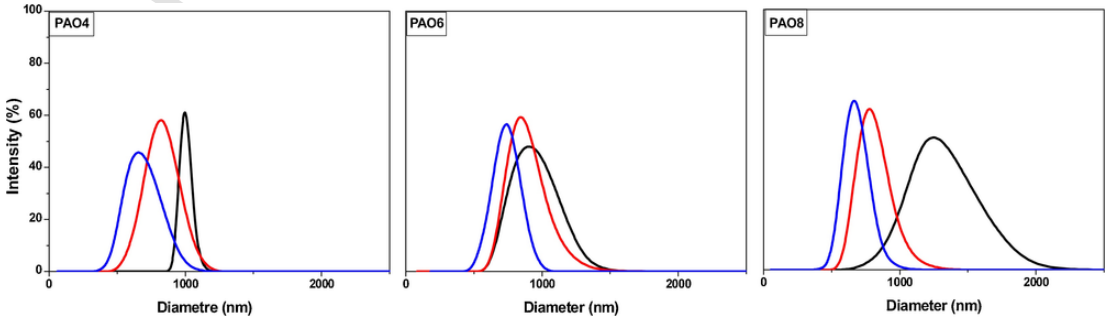

Fig. 5. Size distribution of **s-MoS_2**-based particles as determined by DLS in 3 PAO base oils (PAO4, PAO6 and PAO8): (black) bare **s-MoS_2**, (red) **s-MoS_2-C_8** and (blue) **s-MoS_2-C_{18}**.

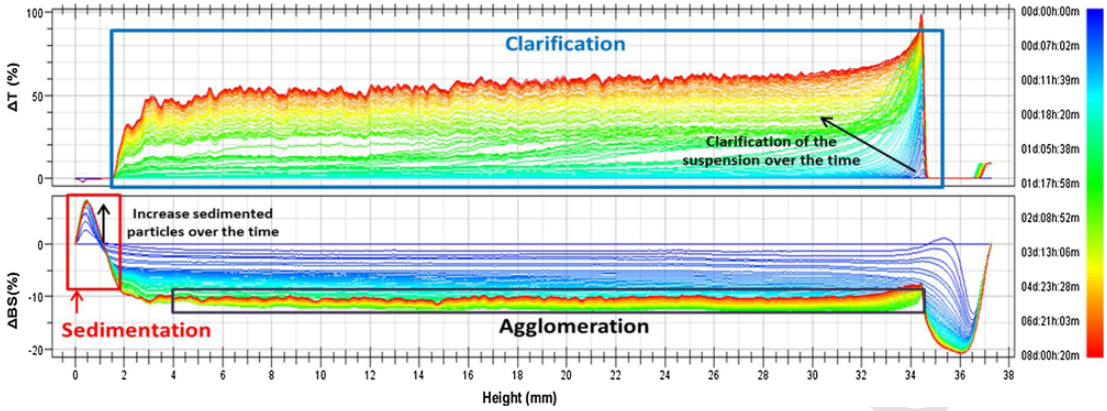

Fig. 6. Typical Δ-transmission (ΔT) and Δ-backscattering (ΔBS) profiles of suspensions of bare s-MoS_2 particles in PAO4 base oil all over the height of the suspension (here 37 mm), and as a function of time. The colours change from blue (at instant 0) to red (at 8 days) (For interpretation of the references to colour in this figure legend, the reader is referred to the web version of this article).

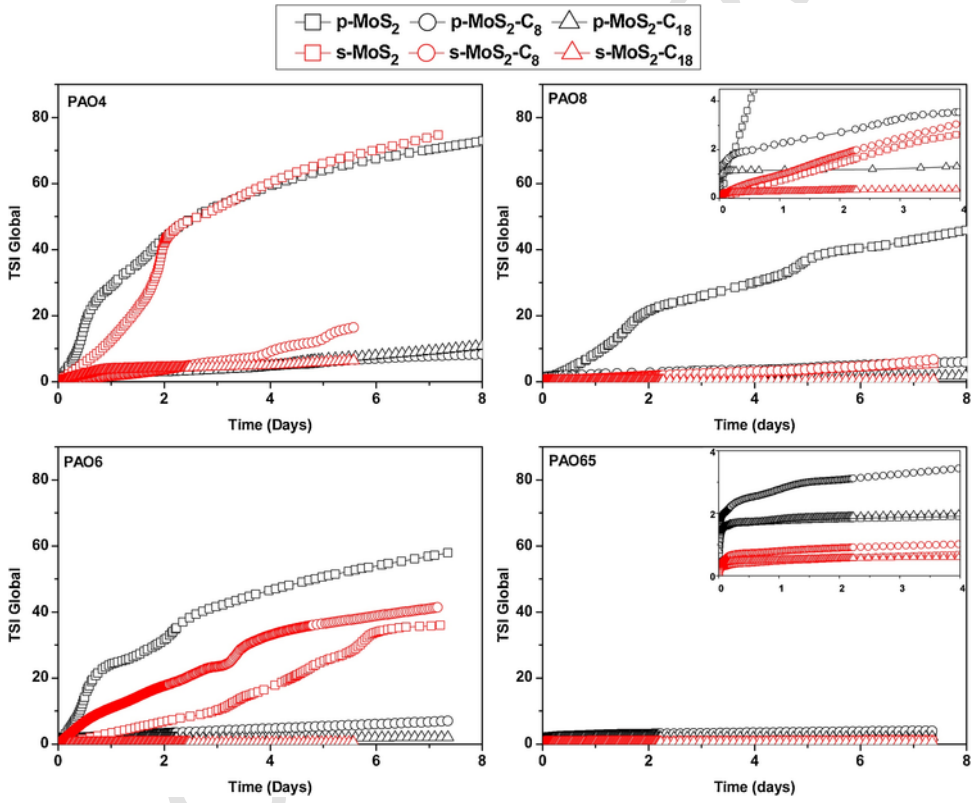

Fig. 7. Variation of TSI values of bare and hydrophobized **s-MoS_2** and **p-MoS_2** in PAO base oils as a function of time.

increase of viscosity, thus evidencing of the stability of the suspensions. For instance, TSI values of bare **p-MoS_2**-based formulations recorded at t = 4 days decreased from 58 in PAO4 to 44 in PAO6 and to 30 in PAO8, whereas the kinematic viscosities of those oils were 34, 66 and 97 cps for PAO4, PAO6 and PAO8, respectively. Moreover, the stability of bare **p-MoS_2**-based formulation dramatically increased (TSI = 2) in PAO65, a highly viscous oil of kinematic viscosity of 1705 cps at room temperature. As a matter of fact, all formulations had roughly similar stability in PAO65 and, after visual inspection, appeared to remain stable for at least 1 year.

On the contrary, in the least viscous oil, PAO 4 kinematic viscosity of 34cps), only the formulations containing functionalized particles with ODTS (C_{18}) were stable for a few days, whereas bare particles sedimented during the first hours. Thus, it can be seen on Fig. 7 that for bare particles formulations in PAO4, TSI values are higher than 50 after 4 days. However, grafting long-chain alkyl moieties on the surface of those particles decreased by at least one decade within the same period. The hydrophobization of the particles not only increased their compatibility with the hydrophobic poly-α-olefin oil, but also reduced the surface energy and thus the attractive forces leading to aggregation. Indeed, better stability was observed for suspensions containing MoS_2 modified with ODTS than with OTS. This can be justified by the length of the hydrocarbon chain of ODTS (C_{18}) leading to a more hydrophobic character than that of OTS (C_8), and therefore increasing the overall hydrophobicity of the grafted MoS_2 surface, hence the higher stability and compatibility with PAO oils. For example, in the case of **s-MoS_2**-based dispersions in PAO4, it can be observed that the TSI decreased with increasing the alkyl chain length from 58 (bare **s-MoS_2**) to 8 (**s-MoS_2-C_8**) and to 5 (**s-MoS_2-C_{18}**). A similar behavior was observed in the other oil phases and also for platelet-like particles. In all

cases, the lowest TSI values (between 1–5) and thus the most stable formulations were obtained for particles functionalized with octadecyl moieties.

Particle shape and size are two other parameters influencing the stability of dispersions. Here platelet-like particles of 1–5 μm were compared with smaller, spherical particles of about 800 nm in diameter. Interestingly, it appears that despite the difference of size, both types of formulations exhibited similar stability. This can be attributed to the effect of MoS_2 particles sizes, apparently, due to higher density of active sites predisposed for adsorption of various species including impurities, which leads to increase the particle weighing, and consequently increase the sedimentation rate [42].The latter can be additionally, enhanced by the drag force exerted depending on the involved particles sizes and shapes. If one defines the drag force F_D applied by the medium (PAO) to the suspended particles as follows: [43]

$$F_D = \frac{1}{2} C_D \rho \omega_S^2 A \quad (2)$$

where C_d is the coefficient of drag, ρ is the density of the fluid, w_s is the velocity settling of particle, and A is the cross-sectional area of the particle, then it can be seen that the drag force depends on the density of the fluid and the coefficient of drag. The density of oils increases from the least viscous, PAO4 to the most viscous, PAO65, while the coefficient of drag depends on the particle shape [44].

Generally, it is well known that the drag force increases as function of projected area which is more important for irregular than spherical shape, especially if this projected area oriented in the direction of fall [41,45]. Thus, the drag force applied to the platelet-like particles is higher than that applied to the spheres, In other words, the displacement of the platelet-like particles is more affected by the drag forces of the medium, and thus their sedimentation rate is reduced with respect to spherical particles. This may explain the convergence of stability despite the difference of particles sizes.

4. Conclusion

Various poly-α-olefins were used as continuous phase to formulate of MoS_2 microparticles-based lubricants. Excellent dispersibility and long-term stability was observed for the particles modified with octadecyl-moieties. The influence on the stability of each parameter of the formulation was highlighted, and revealed that both the viscosity of the base oil and the hydrophobization degree enhance the stability of the dispersions. Interestingly, similar stability was obtained with platelet-like particles up to 5 μm in length as for sub-micrometer spherical particles. Despite the difference in the average size between the particles studied, the stability results could be due to drag forces applied by the lubricating medium on the surface of the particles, which highlights the effect of morphology in improving the stability.

Straightforward applications of those microparticles and their nanoscaled counterparts should be found in tribology and more particularly in intermittent mechanical devices such as wind turbine.

Acknowledgements

The authors acknowledge the institut IRESEN/ Morocco (Project Innowind13 Nanolubricant) for financial support and for the scholarship awarded to MZS.

Appendix A. Supplementary data

Supplementary material related to this article can be found, in the online version, at doi:https://doi.org/10.1016/j.colsurfa.2019.04.003.

References

[1] P. Nagendramma, S. Kaul, Development of eco friendly/biodegradable lubricants: an overview, renew, Sustain. Energy Rev. 16 (2012) 764–774.
[2] W. Winer, Molybdenum disulfide as a lubricant: a review of the fundamental knowledge, Wear 10 (1967) 422–452.
[3] S.V.P. Vattikuti, C. Byon, Synthesis and characterization of molybdenum disulfide nanoflowers and nanosheets: nanotribology, J. Nanomater. 2015 (2015) 1–11.
[4] P. Njiwa, A. Hadj-Aïssa, P. Afanasiev, C. Geantet, F. Bosselet, B. Vacher, M. Belin, T. Le Mogne, F. Dassenoy, Tribological properties of new MoS_2 nanoparticles prepared by seed-assisted solution technique, Tribology Lett. 55 (3) (2014) 473–481.
[5] I. Lahouij, B. Vacher, J.M. Martin, F. Dassenoy, IF-MoS_2 based lubricants: influence of size, shape and crystal structure, Wear 296 (2012) 558–567.
[6] K.H. Hu, M. Liu, Q.J. Wang, Y.F. Xu, S. Schraube, X.G. Hu, Tribological properties of molybdenum disulfide nanosheets by monolayer restacking process as additive in liquid paraffin, Tribol. Int. 42 (2009) 33–39.
[7] M. Gulzar, H.H. Masjuki, M.A. Kalam, M. Varman, N.W.M. Zulkifli, R.A. Mufti, R. Zahid, Tribological performance of nanoparticles as lubricating oil additives, J. Nanopart. Res. 18 (2016) 1–25.
[8] K.H. Hu, Y.K. Cai, X.G. Hu, Y.F. Xu, Synthesis and tribological properties of MoS_2 composite nanoparticles with different morphologies, Surf. Eng. 27 (2011) 544–550.
[9] O. Tevet, P. Von-Huth, R. Popovitz-Biro, R. Rosentsveig, H.D. Wagner, R. Tenne, Friction mechanism of individual multilayered nanoparticles, PNAS 108 (50) (2011) 19901–19906.
[10] M. Akbulut, Nanoparticle-based lubrication systems, J. Powder Metall. Min. 01 (2012) 1–3.
[11] H. Akram, C. Mateos-Pedrero, E. Gallegos-Suárez, N. Allali, T. Chafik, I. Rodriguez-Ramos, A.G. Ruiz, Low solvothermal synthesis and characterization of hollow nanospheres molybdenum sulfide, J. Nanosci. Nanotechnol. 12 (2012) 6679–6685.
[12] P.K. Panigrahi, A. Pathak, Aqueous medium synthesis route for randomly stacked molybdenum disulfide, J. Nanopart. 2013 (2013) 1–10.
[13] Y.H. Lee, X.Q. Zhang, W. Zhang, M.T. Chang, C.T. Lin, K.D. Chang, Y.C. Yu, J.T.W. Wang, C.S. Chang, L.J. Li, T.W. Lin, Synthesis of large-area MoS_2 atomic layers with chemical vapor deposition, Adv. Mater. 24 (2012) 2320–2325.
[14] Syndicat des Énergies Renouvelables, 2015, Septembre.
[15] A. Moshkovith, V. Perfiliev, A. Verdyan, I. Lapsker, R. Popovitz-Biro, R. Tenne, L. Rapoport, Sedimentation of IF-WS_2 aggregates and a reproducibility of the tribological data, Tribol. Int. 40 (2007) 117–124.
[16] A. Moshkovith, V. Perfiliev, I. Lapsker, N. Fleischer, R. Tenne, L. Rapoport, Friction of fullerene-like WS_2 nanoparticles: effect of agglomeration, Tribol. Lett. 24 (2006) 225–228.
[17] S. Kumari, H.P. Mungse, R. Gusain, N. Kumar, H. Sugimura, O.P. Khatri, Octadecanethiol-grafted molybdenum disulfide nanosheets as oil-dispersible additive for reduction of friction and wear, FlatChem 3 (2017) 16–25.
[18] B. Huang, D. Wang, G. Wang, F. Zhang, L. Zhou, Enhancing the colloidal stability and surface functionality of molybdenum disulfide (MoS_2) nanosheets with hyperbranched polyglycerol for photothermal therapy, J. Colloid Interface Sci. 508 (2017) 214–221.
[19] M. Yi, C. Zhang, The synthesis of two-dimensional MoS_2 nanosheets with enhanced tribological properties as oil additives, RSC Adv. 8 (2018) 9564–9573.
[20] F. Lu, H. Du, Z. Chen, X. Zhang, H. Gong, Y. Xue, Stable dispersed MoS_2 nanosheets in liquid lubricant with enhanced rate of penetration for directional well, J. Nanomat. 2016 (2016) 1–8.
[21] C.P. Koshy, P.K. Rajendrakumar, M.V. Thottackkad, Evaluation of the tribological and thermo-physical properties of coconut oil added with MoS_2 nanoparticles at elevated temperatures, Wear 330-331 (2015) 288–308.
[22] J. Sonali, N. Sandhyarani, V. Sajith, Tribological properties and stabilization study of surfactant modified MoS_2 nanoparticle in 15W40 engine oil, IJFMM1 (2014) 1–5.
[23] P. Nallasamy, N. Saravanakumar, S. Nagendran, E.M. Suriya, D. Yashwant, Tribological investigations on MoS_2-based nanolubricant for machine tool slideways, Arch. Proc. Inst. Mech. Eng. Part J J. Eng. Tribol. 1994-1996 229 (2015) 559–567.
[24] S. Aralihalli, S.K. Biswas, Grafting of dispersants on MoS_2nanoparticles in base oil lubrication of steel, Tribol. Lett. 49 (2013) 61–76.
[25] P. Rabaso, F. Dassenoy, F. Ville, M. Diaby, B. Vacher, T. Le Mogne, M. Belin, J. Cavoret, An investigation on the reduced ability of IF-MoS_2 nanoparticles to reduce friction and wear in the presence of dispersants, Tribol. Lett. 55 (2014) 503–516.
[26] H. Shi, X. Fu, X. Zhou, D. Wang, Z. Hu, A low-temperature extraction-solvothermal route to the fabrication of micro-sized MoS_2 spheres modified by Cyanex 301, J. Solid State Chem. 179 (2006) 1690–1697.
[27] A. Kumar, G.D. Thakre, P.K. Arya, L.N.S. Konathala, S. Saran, R. Singh, A.K. Jain, Experimental study on the efficacy of MoS_2 microfluids for improved tribological performance, Arch. Proc. Inst. Mech. Eng. Part J J. Eng. Tribol. 231 (2017) 107–124.
[28] C. Shahar, D. Zbaida, L. Rapoport, H. Cohen, T. Bendikov, J. Tannous, F. Dassenoy, R. Tenne, Surface functionalization of WS_2 fullerene-like nanoparticles, Langmuir 26 (2010) 4409–4414.
[29] M.Z. Saidi, H. Akram, O. Achak, C.E. Moujahid, T. Chafik, N. Canilho, M.J. Stébé, A. Pasc, A.E. Mouakibi, Enhanced dispersibility of MoS_2 nanoparticles in poly-α-olefins lubricant through surface modification, Int. Renew. Sustain. Energy Conf. (2017) 1–5.
[30] M.Z. Saidi, H. Akram, O. Achak, C.E. Moujahid, T. Chafik, N. Canilho, M.J. Stébé, A. Pasc, A.E. Mouakibi, Synthesis of MoS_2 nanoparticles and iImprovement of their dispersibility and stability in PAO base oils, Int. Renew. Sustain. Energy Conf. (2017) 1–6.

[31] Z. Wan, Y. Liu, S. Chen, K. Song, P. Yu, N. Zhao, X. Ouyang, X. Wang, Facile fabrication of a highly durable and flexible MoS_2@RTV sponge for efficient oil-water separation, Colloids Surf. A Physicochem. Eng. Asp. 546 (2018) 237–243.

[32] Z. Wan, D. Li, Y. Jiao, X. Ouyang, L. Chang, X. Wang, Bifunctional MoS_2 coated melamine-formaldehyde sponges for efficient oil–water separation and water-soluble dye removal, Appl. Mater. Today 9 (2017) 551–559.

[33] X. Gao, X. Wang, X. Ouyang, C. Wen, Flexible superhydrophobic and superoleophilic MoS2 sponge for highly efficient oil-water separation, Sci. Rep. 6 (2016) 27207.

[34] H. Akram, O. Achak, S. Haffane, C. Elmoujahid, A. Elmesbahi, D. Elmessoudi, T. Chafik, S. Bensemlali, A. Elmouakibi, Comparison of synthesis routes of inorganic fullerene-like nano-additives for wind turbine lubrication: application of life cycle assessment approach, Proc. Int. Renew. Sustain. Energy Conf., 2014788–790.

[35] P. Afanasiev, I. Bezverkhy, Genesis of vesicle-like and tubular morphologies in inorganic precipitates: amorphous Mo oxysulfides, J. Phys. Chem. B107 (2003) 2678–2683.

[36] R.K. Yuldashev, K.M. Makhkamov, K.T. Sharipov, K.U. Aliev, Synthesis and study by IR and UV methods of spectral analysis of a complex of Mo(VI) with quercetin, Chem. Nat. Compd. 35 (1999) 420–421.

[37] F.A. Miller, C.H. Wilknis, Infrared spectra and characteristic frequencies of inorgnic ions, Anal. Chem. 24 (1952) 1253–1294.

[38] F. Maugé, J. Lamotte, N.S. Nesterenko, O. Manoilova, A.A. Tsyganenko, FT-IR study of surface properties of unsupported MoS_2, Catal. Today 70 (2001) 271–284.

[39] P.A. Gerakines, W.A. Schutte, J.M. Greenberg, E.F. Van Dishoeck, The infrared band strengths of H_2O, CO and CO_2 in laboratory simulations of astrophysical ice mixtures, Astron. Astrophys. 296 (1995) 810–818.

[40] C. Wu, Q. Liu, J. Liu, R. Chen, K. Takahashi, L. Liu, R. Li, P. Liu, J. Wang, Hierarchical flower like double-layer superhydrophobic films fabricated on AZ31 for corrosion protection and self-cleaning, New J. Chem. 41 (2017) 12767–12776.

[41] S.D. Vidyala, W. Asghar, S.M. Iqbal, Porous organic nanolayers for coating of solid-state devices, Int. J. Nanobiotechnology Pharm. 9 (2011) 1–7.

[42] Xianguo Hu, On the size effect of molybdenum disulfide particles on tribological performance, Ind. Lubrication Tribol. 57 (2005) 255–259.

[43] C. Arora, B.P. Kumar, A.C. Narayana, Influence of particle shape on drag coefficient for commonly occuring sandy particles in coastal areas, Int. J. Ocean Clim. Syst. 1 (2010) 99–112.

[44] W.E. Dietrich, Settling velocity of natural particles, Can. Water Resour. J. 18 (1982) 1615–1626.

[45] N. Paul, S. Biggs, J. Shiels, R.B. Hammond, M. Edmondson, L. Maxwell, D. Harbottle, T.N. Hunter, Influence of shape and surface charge on the sedimentation of spheroidal, cubic and rectangular cuboid particles, Powder Technol. 322 (2017) 75–83.